

# INTEGRATED FABRICATION OF SERIALY CONNECTED HIGH VOLTAGE MICROBATTERIES VIA MULTILAYER ELECTRODEPOSITION

Michael Synodis<sup>1</sup>, James Pikul<sup>2</sup>, Sue Ann Bidstrup Allen<sup>1</sup>, and Mark Allen<sup>3</sup>

<sup>1</sup>University of Pennsylvania Department of Chemical and Biomolecular Engineering

<sup>2</sup>University of Pennsylvania Department of Mechanical Engineering and Applied Mechanics

<sup>3</sup>University of Pennsylvania Department of Electrical and Systems Engineering

## ABSTRACT

We report a scheme for the integrated fabrication of MEMS-scale, series-connected battery cells. The approach exploits multilayer electrodeposition of active and sacrificial layers to generate structures that can be formed into high voltage power sources. Aqueous, non-vacuum based fabrication, via electrodeposition, enables high throughput and deterministic control of layer thicknesses and battery performance. Batteries manufactured using this technique offer the potential to match supply voltages to system needs, ranging from conventional electronics to direct drive of high voltage electrostatic or piezoelectric MEMS.

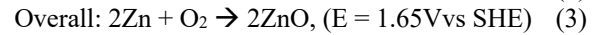
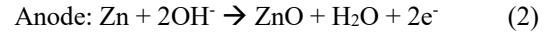
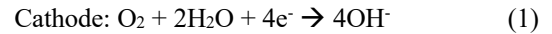
## KEYWORDS

Microbatteries, Zinc-air, Electrodeposition, MEMS, High-voltage power

## INTRODUCTION

The electrical requirements of complex MEMS systems often vary from those of typical circuitry. In such cases, energy storage devices that provide high and/or multiple voltage levels could eliminate the need for up-conversion technologies typically required to operate electrostatic or piezoelectric MEMS<sup>1,2</sup>. Conventional high voltage batteries can be manufactured through external wiring of individually packaged cells, but employing that approach on a smaller scale is electrically challenging and reduces specific performance by adding dead weight to the system<sup>3</sup>. Current state of the art microbatteries can produce high current output and excellent power/energy densities but cannot be scaled or stacked efficiently to achieve the required voltage for many applications<sup>4,5</sup>. Thus, new fabrication approaches are needed to generate serially connected cells (enabling higher voltage outputs) while maintaining intrinsic energy and power density. Designing these approaches around metal-air battery chemistries is ideal, as they have the most promise for achieving high energy densities in a small footprint platform<sup>6,7</sup>. In this study, we utilize multilayer electrodeposition-based fabrication of serial bipolar metal current collectors to enable a zinc-air microbattery with scalable voltage output and potential on-chip device architecture.

Zinc air battery chemistries typically operate with a cell consisting of a pure zinc anode, an alkaline electrolyte, and a porous cathode layer<sup>8</sup>. The cathode layer allows air to diffuse through the cell and enables oxygen reduction at the surface, usually in the presence of a catalyst. The reactions at both electrodes, and overall, are as follows:



There are a few characteristics of zinc-air chemistry that make it easier to integrate into a microbattery architecture compared to other metal-air chemistries. The first is that there is net-zero water consumption, which eliminates the need for a recycling or rehydration system. The second is that gold has been found to act as a catalyst for the oxygen reduction reaction and can therefore be utilized as a structural and catalytic material in the cathode<sup>9</sup>. Lastly, alkaline hydrogel electrolytes have been proven to show high performance delivery of water and hydroxide ions across cells<sup>10,11</sup>. Utilizing a gel-based electrolyte ensures all solid (or pseudo-solid) state materials in the device and reduces the packaging requirements<sup>12</sup>. Thus, a serially integrated zinc-air microbattery can achieve the qualities of high energy density, high voltage, and facile integration with existing MEMS architectures.

## METHODS

In order to achieve scalable voltage outputs in a microbattery platform, a multilayer electrodeposition-based approach is used to generate stacks of serially connected, individual zinc air cells. The fabrication process is described by the schematic in Figure 1.

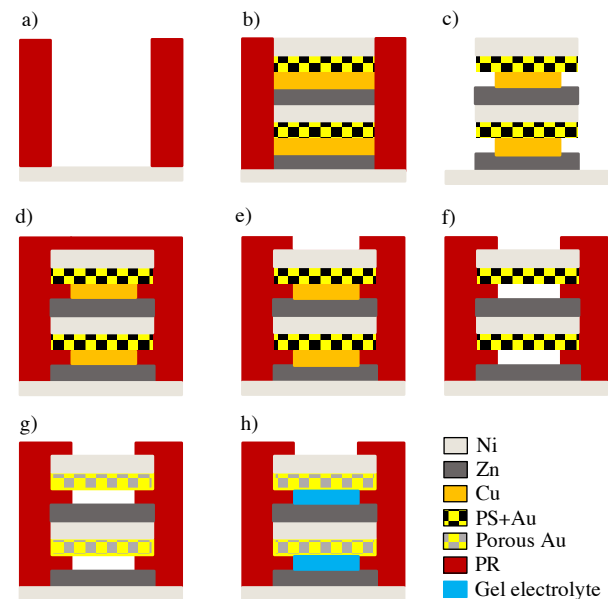


Figure 1: Schematic of the fabrication scheme, highlighting the sequential deposition of active and sacrificial layers, etching to reveal gaps, and infiltration of a hydrogel solid electrolyte.

First, a photoresist (PR) mold (AZ4620, MicroChemicals) is spin cast and developed on the surface of a metal seed layer (Figure 1a). Next, structural and sacrificial cell layers are sequentially deposited. Zinc is first as the anode layer, followed by a sacrificial copper layer for subsequent electrolyte infiltration, then porous gold as the cathode layer, and finally a nickel layer that acts as a bipolar current collector (Figure 1b). The nickel enables electrical connection of the cathode of one cell to the anode of the next cell in the stack. In this study, the zinc deposition occurred in a bath that consists of 35g/L zinc sulfate heptahydrate and 80g/L sodium sulfate, at 10mA/cm<sup>2</sup>. Copper is deposited on top of zinc in two steps. The first stage is an immersion bath of 47 g/L copper sulfate pentahydrate, 52.5 g/L tartaric acid, and 55mL/L ammonium hydroxide. The zinc undergoes a displacement reaction with the copper ions in this solution, forming a barrier layer of copper for subsequent plating. The second step is traditional electroplating from a commercial mirror solution (Grobet) at 10mA/cm<sup>2</sup>. Porous gold is generated first by spray coating a layer of monodisperse, 1 $\mu$ m polystyrene (PS) particles on top of the electrodeposited copper. After sintering at 105°C for 1 hour, a commercial gold sulfite based electroplating solution (Transene) is used to deposit gold through the particles at 4mA/cm<sup>2</sup>. Lastly, a Watts-type nickel electroplating solution consisting of 200 g/L nickel sulfate hexahydrate, 5 g/L nickel chloride hexahydrate, 25 g/L boric acid, and 1 g/L saccharin is used to deposit the nickel current collector at 10mA/cm<sup>2</sup>. All chemicals are from Sigma Aldrich unless otherwise specified. This set of four layers (six steps) is repeated until the desired number of cells in the stack has been reached.

After the layers for a full stack were deposited, the AZ4620 mold was removed and the copper layers were etched back slightly to reveal gaps at the edges (Figure 1c). A second photoresist mold (SU-8, MicroChemicals), was then deposited and exposed to anchor the multilayer stacks in the holes where the first mold and copper previously occupied (Figure 1d, 1e). Subsequently, the remaining copper and PS sacrificial materials are etched completely, revealing a gap between the zinc and gold layers for electrolyte intrusion as well as pores in the gold cathodes for air diffusion (Figure 1f, 1g). Copper etch is performed using a neutral pH etchant that is selective for copper over nickel and zinc (Transene), and the PS etch is completed in toluene. Lastly, a polyvinyl alcohol (PVA) and potassium hydroxide (KOH) based gel electrolyte is infiltrated into the gaps to complete the fabrication (Figure 1h). A solution of 1g PVA/10mL DI water is mixed with an equivalent volume of 1M KOH solution. After mixing for several hours, the solution is drop cast and infiltrated into the suspended layered structures via gravity and capillary force. Upon full coverage, the structure is dried in a vacuum oven at 95°C.

## RESULTS AND DISCUSSION

The zinc-air, all electroplated microbatteries were analyzed by assessing each fabrication step with optical and scanning electron microscopy, followed by electrochemical characterization via galvanostatic discharge tests. Figure 2 highlights microscopic images of the device fabrication at various stages of completion.

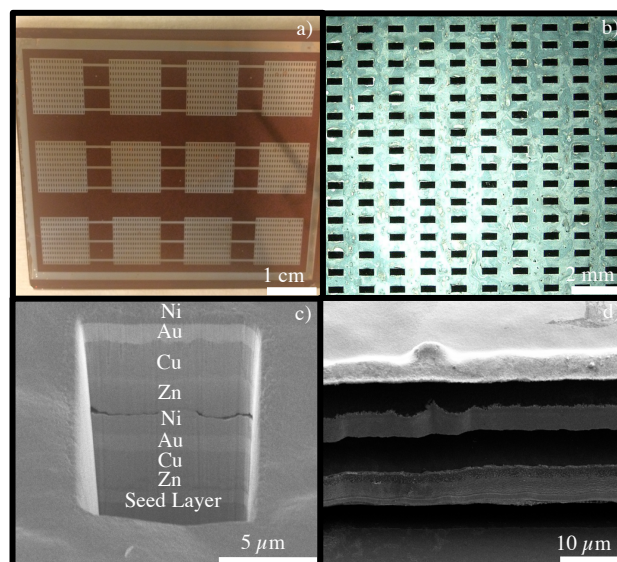


Figure 2: Optical and SEM images of batteries mid fabrication: a) Optical image of patterned battery molds on seed layer. b) Top down optical image of layer stacks after first mold removal. c) Cross sectional SEM image of interlayer interfaces after electrodeposition. d) Cross sectional SEM image of suspended layers after sacrificial Cu etch.

In Figure 2a, a top down, optical image of the stacks is shown on the carrier substrate. Twelve 1x1cm batteries can be achieved on a single substrate, where each were be used to carry out electrochemical testing at various current densities. Figure 2b shows a top down view of the top nickel current collector after stack deposition and removal of the first PR mold. Figure 2c is an SEM image of a two-cell stack sectioned via a focused ion beam. The uniform interfaces indicate good compatibility between the five deposition solutions as well as tunable layer thicknesses achieved by altering the deposition times. Lastly, Figure 2d is an SEM image of stacked layer cross sections after etching of the sacrificial materials (copper and polystyrene). This image highlights the suspended, micron level gaps between the zinc anode and porous gold cathode layers within each cell, where the hydrogel electrolyte is infiltrated.

A critical piece of the fabrication process that ensures both individual cell operation as well as the ability to scale voltage is the deposition of the porous gold cathode layers. Figure 3 demonstrates the methodology of generating the porous films. First, in Figure 3a, a top-down SEM image of the PS particle spray coating and packing is shown. The particles in this image have been dried but not sintered, so the individual particles can be identified. The packing is random and non-uniform, but once sintered the particles will create a continuous network through which gold can be electrodeposited, which is shown in Figure 3b. For demonstration, the gold is slightly over-plated on top of the mold. Figures 3c and 3d show the introduction of pores in the gold film after the PS particles have been etched in toluene and the regeneration of a solid surface for subsequent cell stacking by continuing plating over the top of the PS.

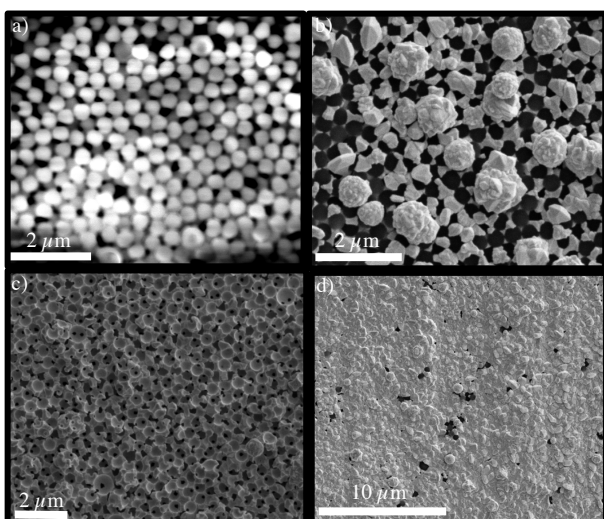


Figure 3: SEM images of particle template and electrodeposition of gold cathode: a) Particles after sintering. b) Gold strike through template c) Particle etch to reveal porous layer d) Planarization of the surface

While Figure 3 highlights the cathode structure as it is built from the top down, Figure 4 shows a cross section of a bipolar current collector interface. In this SEM image, which was generated via focused ion beam milling, zinc, nickel and porous gold layers have been deposited. The bottom-most layer is zinc, the middle layer is the nickel current collector, and the top layer is the porous gold. Continuing the fabrication process from here would require infiltrating gel above the gold layer and below the zinc layer. The zinc here shows slight cracking due to the stress of nickel deposition on top.

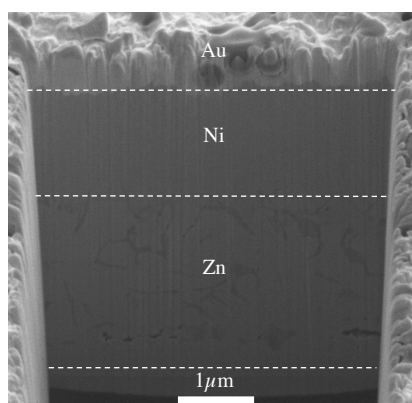


Figure 4: FIB SEM Cross Section of a sample Zn, Ni, Porous Au interface

In the gold layer, pores generated by the PS spray coating will act as conduits for oxygen diffusion and ideally allow reaction to occur throughout the thickness and length of the cathode. Since the oxygen reduction reaction is the slowest kinetic step in the operation of the battery, it is critical that these pores permeate the entire layer to provide maximum mobility for oxygen and the largest surface area possible for reactions to take place.

After the fabrication of the stacked batteries was completed, electrochemical testing was conducted through galvanostatic discharge. These tests verified the scaling of voltage through the series connection of cells

via the bipolar nickel current collector and tested for the fractional utilization of the electrodeposited zinc anode layers during the discharge of the battery. Gravimetric and volumetric energy and power densities were also calculated using these discharge curves. Figure 5 displays sample discharge curves for a single-cell and two-cell battery stack.

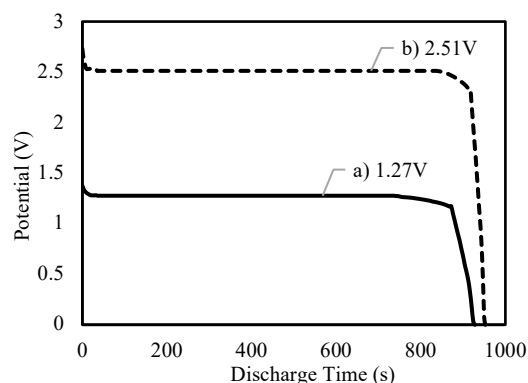


Figure 5: Sample discharge curves for two fabricated batteries. a) A single cell electroplated system, and b) A two-cell electroplated battery stack

In curve a, the single cell battery achieves a discharge plateau voltage of 1.27V, and in curve b the two-cell stack discharge voltage is 2.51V. This indicates that the voltage does scale through the integrated nickel current collector, but it is not exactly double due to increases in internal resistances as the number of electroplated layers increases. Additionally, there are slight variances from battery to battery during fabrication.

Discharge curves were collected and analyzed for batteries with two footprint dimensions, 1x1cm and 0.5x0.5cm, resulting in areas of 1cm<sup>2</sup> and 0.25 cm<sup>2</sup>, respectively. The varied footprint area systems were built to highlight the versatility of the fabrication scheme as well as provide insight into how the aspect ratio of the battery layers affects the hydrogel electrolyte infiltration depth as well as oxygen diffusion through the battery during discharge. The performance characteristics of each battery size were compiled and summarized in Table 1, where the large area column refers to batteries fabricated with a 1cm<sup>2</sup> footprint, and the small area column refers to batteries fabricated with a 0.25cm<sup>2</sup> footprint.

Table 1: Performance data for large and small footprint zinc-air microbatteries

Parameter (Units)	Large A	Small A
Number of cells	2	2
Total height (μm)	20	20
1C Discharge voltage (V)	2.51	2.47
Power Density (W/L)	1277	1400
Energy Density (Wh/kg)	211	250
Energy Density (Wh/L)	531	741
Capacity (mAh)	0.42	0.14

While the number of cells and voltages remained similar for the small and large platforms, the power and energy densities both increased for the small platform. It is hypothesized that this is due to more efficient transport

of both gel electrolyte and oxygen through the smaller aspect ratio paths in the fabrication and discharge processes, respectively. All material diffusion during battery construction and use is limited to being initiated from the edges, so optimizing the layer thicknesses and transport lengths via the battery footprint will have a large impact on future battery performance. Edge based diffusion and infiltration is necessary to prevent cell to cell electrolyte connection within the stack, which would short out the cells and eliminate the voltage scaling. This is why anchors are necessary to provide suspended gaps during fabrication, and why they must permanently remain in the device once developed.

Rate performance for the stacked batteries was investigated by varying the applied discharge current from 0.1C to 2.5C, where xC represents the current needed to discharge the battery completely in  $x^{-1}$  hours, according to the theoretical capacity of the zinc layers in the stack. Figure 6 shows how the capacity of both large and small footprint area devices changes as a function of the discharge rate applied.

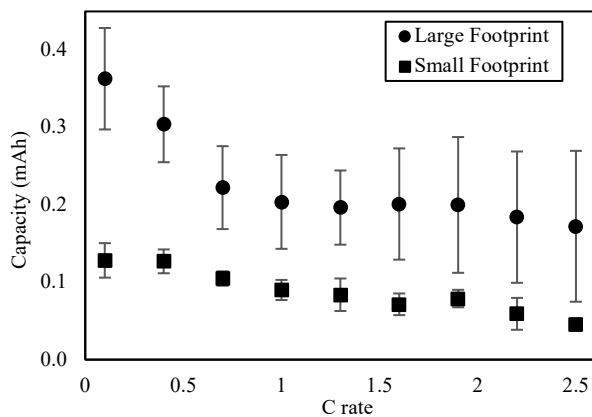


Figure 6: Microbattery capacity as a function of discharge rate, for small and large footprint architectures.

It can be seen that as the rate increases above  $\sim 1C$ , the capacity drops, indicating that a diffusion limited region is reached. The oxygen depletion rate due to the ORR at the gold interface is faster than the diffusion rate through the porous structure. At that point, a larger amount of the zinc mass in the battery cannot be utilized. Thus, the batteries would best perform for direct drive of low current, higher voltage operations.

## CONCLUSIONS

In this work a fabrication approach for the development of solid state, multi-cell zinc air battery stacks was demonstrated. The series electrical connection between cells in the stacks was enabled by a multilayer electroplating technique for the sequential deposition of anode, cathode, current collector, and sacrificial metal layers, followed by etching and infiltration of an alkaline hydrogel electrolyte. Proof of concept batteries show voltage scaling with limited changes in energy performance, and battery footprint areas have been adjusted to increase energy and power density metrics. This approach shows promise for further increases in

voltage outputs and integration with MEMS based actuation systems.

## ACKNOWLEDGEMENTS

Funding for this research was supported by DARPA, under grant# HR001119C0039. The research was partially carried out in the Singh Center for Nanotechnology, which is supported as part of the NNCI by NSF grant NNCI-1542153.

## REFERENCES

- [1] D. Steingart. "Power sources for wireless sensor networks." *Energy harvesting technologies*. Springer, Boston, MA, 2009. 267-286.
- [2] K. Cook-Chennault, N. Thambi, and A. Sastry. "Powering MEMS portable devices—a review of non-regenerative and regenerative power supply systems with special emphasis on piezoelectric energy harvesting systems." *Smart materials and structures*. 17.4 (2008). 043001.
- [3] Y. Wang, B. Liu., Q. Li, S. Cartmell, S. Ferrara, D. Deng, and J. Xiao. "Lithium and lithium ion batteries for applications in microelectronic devices: A review." *Journal of Power Sources*, 286 (2015), 330-345.
- [4] N. Kyeremateng and R. Hahn. "Attainable Energy Density of Microbatteries." *ACS Energy Letters* 3.5 (2018), 1172-1175.
- [5] J. Pikul, J. Liu, P. Braun, W. King. "Integration of high capacity materials into interdigitated mesostructured electrodes for high energy and high power density primary microbatteries." *Journal of Power Sources* 315 (2016): 308-315.
- [6] M. Rahman, X. Wang, and C. Wen. "High energy density metal-air batteries: a review." *Journal of The Electrochemical Society* 160.10 (2013): A1759-A1771.
- [7] J. Lee, S. Kim, R. Cao, N. Choi, M. Liu, K. Lee, and J. Cho. "Metal-air batteries with high energy density: Li-air versus Zn-air." *Advanced Energy Materials* 1.1 (2011): 34-50.
- [8] J. Fu, Z. Cano, M. Park, A. Yu, M. Fowler, and Z. Chen. "Electrically rechargeable zinc-air batteries: progress, challenges, and perspectives." *Advanced materials* 29.7 (2017): 1604685.
- [9] R. Zeis, T. Lei, K. Sieradzki, J. Snyder, and J. Erlebacher. "Catalytic reduction of oxygen and hydrogen peroxide by nanoporous gold." *Journal of Catalysis* 253.1 (2008): 132-138.
- [10] G. Wu., S. Lin, and C. Yang. "Alkaline Zn-air and Al-air cells based on novel solid PVA/PAA polymer electrolyte membranes." *Journal of Membrane Science* 280.1-2 (2006): 802-808.
- [11] A. Mohamad. "Zn/gelled 6 M KOH/O<sub>2</sub> zinc-air battery." *Journal of power sources* 159.1 (2006): 752-757.
- [12] V. Caramia and B. Bozzini. "Materials science aspects of zinc-air batteries: a review." *Materials for Renewable and Sustainable Energy* 3.2 (2014): 28.

## CONTACT

\*Michael Synodis, Email: msynodis@seas.upenn.edu